PV Asia Pacific Conference 2012

Microstructural Analysis of Crystal Defects Leading to Potential-Induced Degradation (PID) of Si Solar Cells

Volker Naumann[a,*], Dominik Lausch[a], Stephan Großer[a], Martina Werner[a], Sina Swatek[a], Christian Hagendorf[a], Jörg Bagdahn[a,b]

[a]*Fraunhofer Center for Silicon Photovoltaics CSP, Walter-Hülse-Str. 1, 06120 Halle (Saale), Germany*
[b]*Anhalt University of Applied Sciences, Photovoltaic Materials, Bernburger Str. 57, 06366 Köthen (Anhalt), Germany*

Abstract

A monocrystalline Si solar cell with a low corrugation front side texture was processed to a mini module and has been stressed under potential-induced degradation (PID) conditions. Subsequently, a sample delaminated from PID-affected area has been prepared and investigated down to the microscale employing SEM/EBIC, ToF-SIMS depth profiles and TEM at defect structures. The electrical shunts resulting from PID are confirmed to be locally distinct and coincide with Na aggregations in the antireflective coating (ARC). Moreover, by means of EBIC and TEM measurements these shunts are found to be spatially associated to structural defects within the silicon crystal.

1. Introduction

Potential-induced degradation (PID) of crystalline Si solar cells is intensively investigated since first publications more than two years ago [1, 2]. It has a strong detrimental impact on module reliability due to a massive power loss by shunting of cells [3]. In the last years there has been a concentration on

---

* Corresponding author. Tel.: +49 345 5589-119; fax: +49 345 55 89 101
E-mail address: volker.naumann@csp.fraunhofer.de

material investigations including studies of the influence of antireflective coating (ARC) refraction index, encapsulant materials, glass variation or doping of the solar cells [2, 4]. Approaches for preventing PID are derived on system-, module- and cell level and are already partly being applied in production. However, the origin of PID on a microstructural level is still unclear. Recent papers [5, 6] prove that the drift and distribution of Na is responsible for potential-induced shunts. Moreover there are evidences that the induced shunts are individually spread over PID-affected cell regions [6]. The aim of this study is to substantiate the correlation between shunts and the distribution of Na within the ARC layer. Furthermore structural reasons for the position of particular resident potential-induced shunts shall be identified.

2. Experimentals

The degradation of mini modules is performed in a climate chamber at damp heat conditions (85 °C, 85% relative humidity). The front glass of mini modules is covered with aluminium foil, which is connected to a high positive voltage while the cell remains on earth potential.

Electroluminescence (EL) images of the mini module have been acquired with a coolSamBa HR-830 Si camera. For further investigations on the cell it is required to detach cell fragments from the front EVA/glass compound. A dark lock-in thermography (DLIT) setup by Thermosensorik, equipped with an InGaAs detector, has been used to localise shunts on a micrometer scale.

The encountered shunts have been imaged by scanning electron microscopy (SEM) and electron beam induced current (EBIC) with a SU-70 (Hitachi) with lock-in EBIC system DISS 5 EBIC by point electronic. The electron beam energy for SEM and EBIC has been varied between 3 and 30 keV.

The chemical information at shunt positions, i.e. 3D distribution of Na, has been measured by time-of-flight secondary ion mass spectroscopy (ToF-SIMS) within a TOF.SIMS 5 by IONTOF with a pulsed Bi primary ion beam scanning over the sample surface. ToF-SIMS depth profiling uses an additional O_2^+ (1 keV) sputter beam for planar erosion of surficial layers.

Cross sections have been prepared at shunt positions by focused ion beam (FIB) and further imaged by SEM/EBIC. Cross-sectional lamellae of defect positions have been imaged by transmission electron microscopy (TEM) in Tecnai (FEI) and CM20 (Philips) instruments.

3. Results

A monocrystalline silicon solar cell (156×156 mm^2) with a flat alkaline textured front side was soldered with contact ribbons and laminated to a soda lime glass pane using standard EVA encapsulants and a PVF back sheet. This layout is equivalent to standard solar modules. The obtained mini module was degraded for 24 hours with an aluminium foil on the glass front side (bias +600 V) and grounded cell contacts while it was exposed to an environment of 85 °C and 85% relative humidity. For reference about 20% of the solar cell remained non-degraded since the cell was not completely covered with foil.

3.1. Electrical characterisation and shunt localisation

After degradation an EL image of the mini module (Fig. 1a) is acquired in order to monitor the degree

of degradation and to find a suitable position for delamination. It reveals shunted regions centered between the busbars. A shunt resistance of ~1200 Ωcm^2 has been measured at the PID-affected mini module (Fig. 1b). This is a comparably high resistance with respect to recent experiments performed with a multicrystalline Si cell with a special PID-prone ARC layer [6]. However, a distinct ohmic behaviour of the cell is indicated by the linear I-V characteristic at reverse bias. A piece of the cell with a size of 1.5×1.5 cm^2 was detached from the front side EVA/glass compound in a region with low EL signal, i.e. low shunt resistance. The following results have been obtained at this delaminated shunted fragment of the cell.
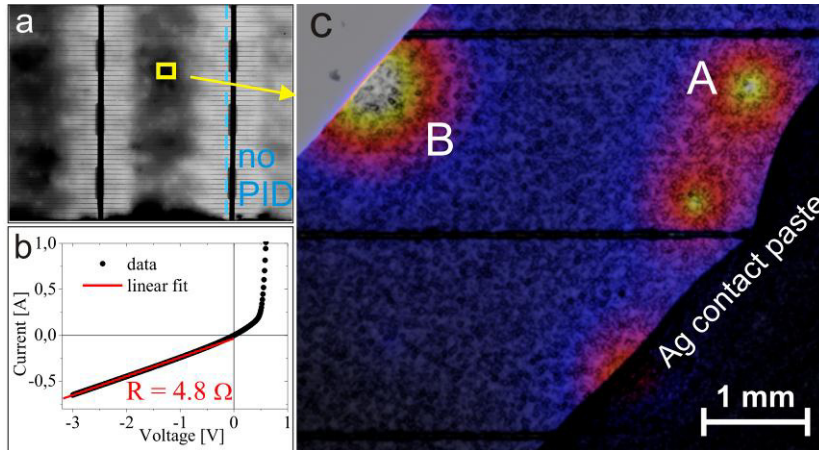

Fig. 1. (a) EL-image of a part of the mini module after degradation. (b) Dark I-V curve of the mini module. (c) DLIT amplitude (5 V in reverse bias, 7 mA, 25 Hz) + topography overlay image of a delaminated cell fragment with a number of shunts originating from PID. Shunts A and B are used for ToF-SIMS and FIB/TEM investigations, respectively.

The delaminated fragment is homogeneously contacted with an additional "busbar", made with Ag contact paste on the front side. First, DLIT images have been acquired at this sample in order to investigate the distribution of shunts. The image in Fig. 1c reveals local shunts with a density of approximately ten per square centimeter. Obviously, these shunts develop only in regions where a high voltage has been applied to the mini module as can be concluded from the EL overview in Fig. 1a (right hand side marked "no PID"). This proves findings of a recent work [6], but with a much smaller density of shunts. The piece that is shown in Fig. 1c exhibits a shunt resistance of roughly 600 Ωcm^2. High resolution DLIT images (not shown here) reveal shunt diameters well below 30 μm. Compared to the relatively low density of shunts this indicates high shunt current densities of >10 A/cm^2 at the open-circuit voltage. A number of encountered shunts are chosen for detailed microstructure investigations. In the following, referring to Fig. 1c, SEM/EBIC and ToF-SIMS results are shown at shunt A whereas shunt B is an example where a cross section has been imaged by SEM/EBIC and TEM.

3.2. SEM and ToF-SIMS investigations

Individual shunts of Fig. 1c are identified by SEM using EBIC. Shunts, particles and recombination active regions reduce the EBIC signal locally. Regarding to the low density of shunts on this sample they are studied as separate objects. Figure 2 shows the shunt marked with "A" in Fig. 1c. The secondary

electron (SE) image in Fig. 2a clearly shows that there is no particular feature visible at the surface where the EBIC signal (Fig. 2b) is drastically reduced. Furthermore the dark spot in the EBIC image is not circular, which indicates that the shunt is not dot-like. The long axis of the shunt appears to be oriented along a <110> direction. Beside the <110>-orientated structures of the truncated pyramids and small pyramids, the surface is free of any structural inhomogeneities or contaminations related to the shunt position.
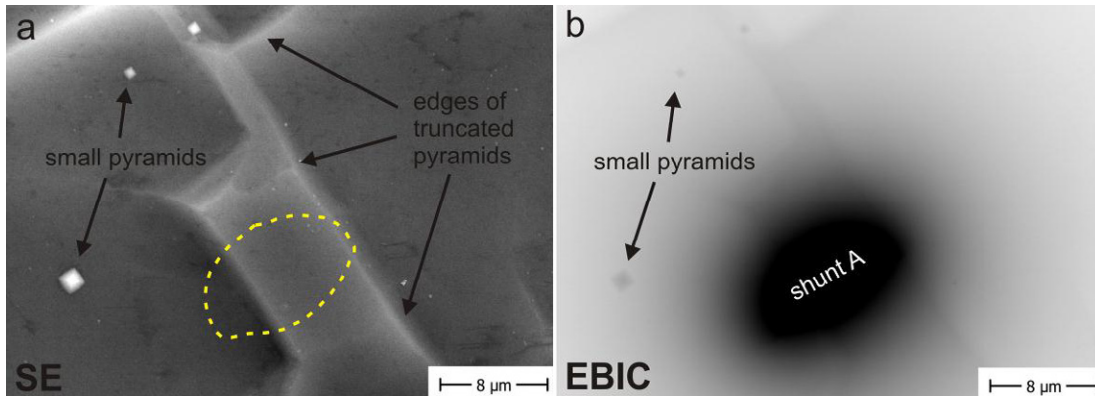

Fig. 2. SEM images of shunt A. The SE image (a) exhibits no particular feature visible at the surface, where the EBIC image (b) shows an extended area with low signal at the corresponding position.

Up to this point there is no indication what kind of defects may cause the shunts. From recent works it is known that potential-induced shunts are correlated to accumulation of Na at the SiN/Si interface [5, 6]. This sample is very suitable for substantiating this fact, because the delaminated solar cell fragment has a mostly flat and clean surface that is only intermitted by edges of truncated pyramids. With this it is possible to clearly identify individual buried accumulations of Na with adequate lateral and depth resolution.

For mappings of chemical information at shunt sites ToF-SIMS is employed using a pulsed Bi^+ ion beam scanning over an area of $500 \times 500\ \mu m^2$. Positively charged ions are measured. Since only the uppermost nm of the sample surface contributes to the signal within an ion map, the sample surface is gradually eroded between sequenced surface mappings by a second more intense O_2^+ sputter beam that is scanned over a larger area ($700 \times 700\ \mu m$). Ion maps of selected species integrated over a certain depth or depth profiles integrated over a certain area are reconstructed from ToF-SIMS raw data sets.

Figure 3a shows a reconstruction of the measured Na intensity (green colour) near the SiN/Si interface at the potential-induced shunt A. The total ion image (comprises all registered secondary ions) is overlaid in red color for topological information. The position marked with "ROI" equals the location of shunt A in the EBIC image (inset of Fig. 3a). It is obvious that the strongest accumulation of Na is exactly at the same position of the shunt. Other small aggregations of Na (green) arise mainly from local surface contaminations that are sputtered continuously on top of the SiN layer during depth profiling. Figure 3b shows the reconstruction of the depth profile only within the ROI (white circle in Fig. 3a). The depth profile reveals that the Na accumulation is detected within a close depth interval directly at the interface

between the SiN ARC layer and the Si substrate. These results have been confirmed at other shunt positions, too.
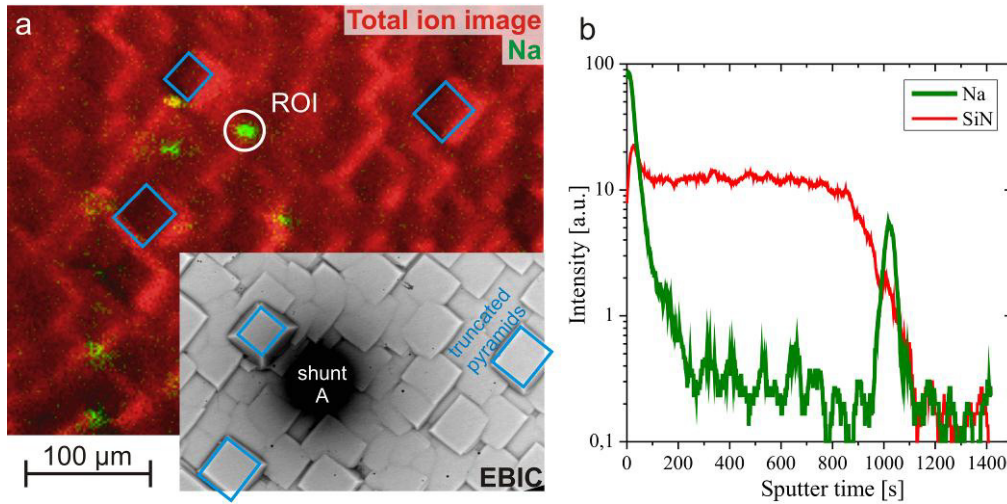

Fig. 3. (a) ToF-SIMS ion image at shunt A with topography information in the total ion image (red) and distribution of Na (green). The inset shows the corresponding EBIC image acquired the ToF-SIMS measurement at exactly the same position. Blue squares indicate the same positions in ToF-SIMS and EBIC image. (b) Depth profile of the SiN^+ and Na^+ intensities throughout the SiN layer evaluated within the white marked region of interest (ROI).

It has been found by means of subsequent DLIT investigations that the shunt intensities of individual shunts are reduced even if only a fraction of the SiN layer is removed by ion sputtering. The same had been observed after gradual removal of SiN by chemical etching at another PID-affected cell fragment (not shown here).

3.3. SEM/EBIC and TEM investigations at cross-sections

In order to localise defects within the Si material which may support the creation of local shunts during the PID process, cross sections have been prepared by FIB technique at three shunts. For this purpose the FIB instrument has been equipped with a portable EBIC system. FIB milling has been started several μm in front of the shunt. Thin Pt layers are deposited on the sample surface to protect the upper edge of the final cross section from parasitic erosion. Then the cross section has been driven parallel towards the shunt position visible in EBIC.

A cross-sectional SEM view of shunt B is shown in Fig. 4. The SE image (Fig. 4a) is inconspicuous except for small silicon pyramids on the wafer surface. The corresponding EBIC image (Fig. 4b) of the cross section reveals a well-defined p-n junction that is weakened over a length of ~10 μm. This has been expected from the top view LIT and EBIC results. However, beyond that, discrete structures with drastically reduced EBIC signal appear inside the Si bulk material, just below the location of the weakened p-n junction – at a depth of 0 to 4 μm below the emitter region (see Fig. 4b). A tilted defect line in the Si bulk is found by EBIC at every investigated cross section of PID-shunted locations. Always, directly above these lines and also between the line and the emitter layer, regions without any EBIC

signal (black) can be found. In general, only the EBIC images show these features while no structural abnormalities are visible in SE images.
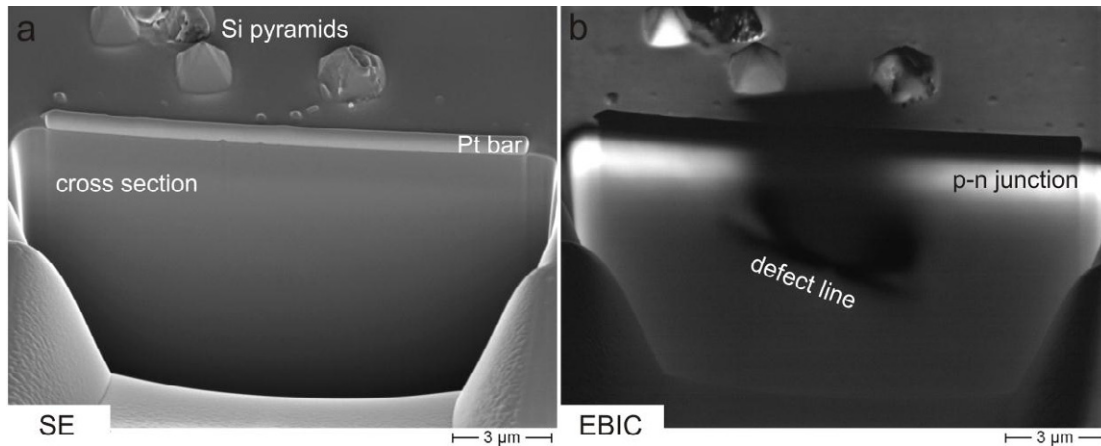

Fig. 4. Cross-sectional SEM view of a shunt position. The SE image (a) exhibits no visible structural defects. The corresponding EBIC image (b) shows a disturbed p-n junction and distinct linear regions with low signal both in cross section and on the surface.

Top-view EBIC images have been acquired with comparatively low beam energy of 3 keV having an enhanced lateral resolution and surface sensitivity. Roughly 4 µm long lines with reduced EBIC intensity are found on the solar cell surface at every of the three investigated shunts. The dark lines on the surface are always parallel to the base edge of (truncated) pyramids which corresponds to a <110> direction. Furthermore, the cross section of shunt B (Fig. 4b) shows also a rectangular region (black) with reduced EBIC signal in front of the dark line, i.e. between the dark line on the surface and the tilted line visible in the cross section.

Two of the investigated cross sections have been further prepared by FIB to finally obtain electron transparent lamellae with a thickness of ~100 nm. In TEM images structural details, which could not be resolved by SEM, become visible.

The TEM image in Fig. 5a shows a part of a cross section as treated above. Residues of the Pt cover and the ~80 nm thick SiN layer are clearly visible in the upper part. The dark bowed stripes within the Si are attributed to diffraction phenomena resulting from warping and thickness inhomogeneity of the lamella. The straight defect line in the middle of the lamella has the same tilt angle and relative position as the dark feature in the corresponding EBIC image shown above. It is concluded from comparative measurements at two shunt locations that defect lines in both EBIC and TEM images represent the same features. They are clearly assigned to crystallographic defects – most probably stacking faults.

Figure 5b shows how the present situation at the shunt sites is imagined: The plane of the cross section is drawn grey. The red line is the intersection line between the cross section plane and the (111) plane parallel to a side face of a pyramid. (001) and (110)-planes are drawn for orientation. Transferred to TEM images the tilted double line is present where the stacking fault in a {111} plane (parallel to a side face of pyramids) breaks through the "front" and "rear" surfaces of the cross-sectional lamella. The defect line

would appear parallel to the surface if a TEM lamella would be prepared exactly parallel to the base edge of Si pyramids, e.g. in a {110} plane. The tilt angle φ of the defect line with respect to the surface has been calculated as a function of the angle α between plane of the cross section and the (110) plane. This calculation supports the assumed model since the measured angles φ and α go well together, respectively.
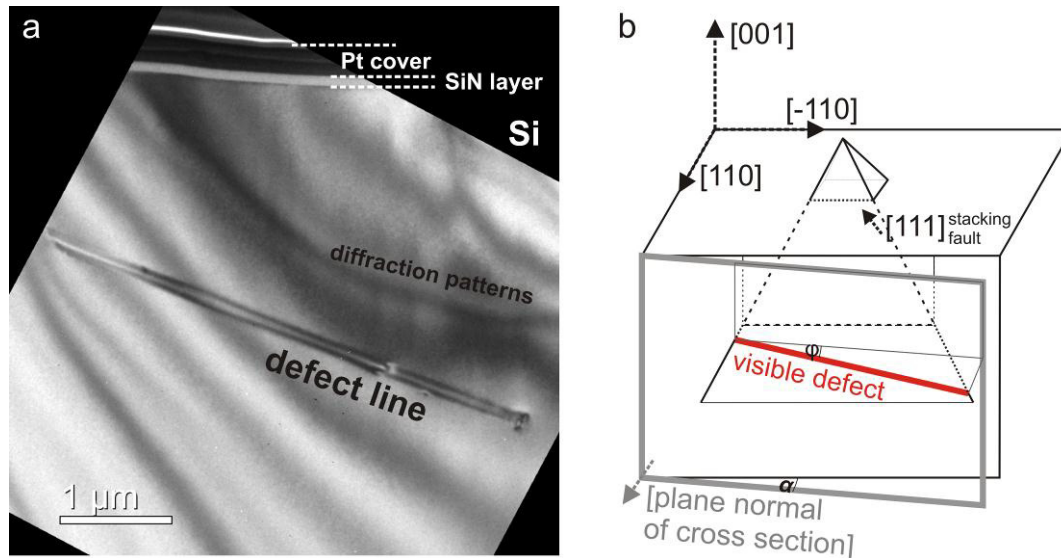

Fig. 5. (a) TEM image of a cross section where EBIC revealed a strongly disturbed region before. (b) Diagram of a stacking fault in a {111} plane that crosses a TEM lamella.

4. Discussion

Previous results obtained at a highly PID-prone multicrystalline Si solar cell [6] could be qualitatively reproduced and furthermore substantiated at this sample with low shunt density: After degradation the cell shows ohmic behaviour which correlates to broadened shunted areas visible in EL images[†]; local shunts are resolved by DLIT at higher resolution and are also detectable by EBIC; in SEM the surface of shunted areas shows no structural defects; but there are distinct Na accumulations measured by ToF-SIMS near the SiN/Si interface exactly at shunt locations.

In a simple consideration the last point is striking since already a partial removal of the SiN layer by ion sputtering or chemical etching results in significantly reduced shunt intensity. The question on how PID shunts can be affected by shallow etching of the SiN layer while Na aggregations are found deeper at the SiN/Si interface will be part of future investigations.

Nevertheless, the fact that all of three investigated shunt sites reveal extended defects inside the Si

---

[†] Therefore the term "potential-induced shunting PIS" as introduced in [7] should be preferred to "PID" which comprises also other degradation effects.

bulk is of striking significance. From the current measurements it is known that the shape of the reduced EBIC signal correlates with shape, location and orientation of stacking faults in {111} planes that intersect the p-n junction and reach the surface. Stacking faults are considered to be present at corresponding positions already before degradation. During PID their presence seems to attract Na ions which accumulate in close proximity. The main question that arises is how stacking faults, which reach the surface, can be modified by the flow of Na ions so that a conductive channel through the p-n junction is formed.

From our current results it is not clearly deducible whether the proposed model of PID-shunting presented in [6] is supported or not. On that account further investigations dealing with ultimate spatial resolution and combined elemental analysis capabilities are planned.

5. Summary

The parallel resistance of a PID affected cell is reduced due to a number of localised shunts. The investigated shunt positions exhibit coinciding local Na accumulations at the SiN/Si interface. Cross sectional views reveal that all investigated potential-induced shunts are associated with crystallographic stacking faults which intersect the p-n junction and reach the surface. The main questions for forthcoming investigations will be related to the accumulation process of Na ions drifting through the SiN layer towards crystallographic defects finally leading to shunting of the p-n junction.

Acknowledgement

References

[1] Pingel S, Frank O, Winkler M, Daryan S, Geipel T, Hoehne H *et al. Potential Induced Degradation of solar cells and panels. Proc. 35th IEEE Photovoltaic Specialists Conf.*, USA, 2010, pp. 2817–2822.

[2] Berghold J, Frank O, Hoehne H, Pingel S, Richardson B, Winkler M. Potential Induced Degradation of solar cells and panels. *Proc. 25th European Photovoltaic Solar Energy Conf.*, Valencia, Spain, 2010, pp. 3753-3759.

[3] Hacke P, Smith R, Terwilliger K, Glick S, Jordan D, Johnston S *et al.* Testing and analysis for lifetime prediction of crystalline silicon PV modules undergoing degradation by system voltage stress. *Proc. 38th IEEE Photovoltaic Specialists Conf.*, Austin, USA, 2012, pp. 1750-1755.

[4] Hacke P, Kempe M, Terwilliger K, Glick S, Call N, Johnston S *et al.* Characterization of multicrystalline silicon modules with system bias voltage applied in damp heat. *Proc. 25th European Photovoltaic Solar Energy Conf.*, Valencia, Spain, 2010, pp. 3760–3765.

[5] Naumann N, Hagendorf C, Großer S, Werner M, Bagdahn J. Micro structural root cause analysis of potential induced degradation in c-Si Solar Cells. *Energy Procedia* 2012;**27**:1-6.

[6] Bauer J, Naumann V, Großer S, Hagendorf C, Schütze M, Breitenstein O. On the mechanism of potential-induced degradation in crystalline silicon solar cells. *Phys. Status Solidi RRL* 2012; **6(8)**:331–3.

[7] Taubitz C, Schütze M, Köntopp MB. Towards a kinetic model of potential-induced shunting. *Proc. 27th European Photovoltaic Solar Energy Conf.*, Frankfurt, Germany, 2012, pp. 3172-3176.